Circuit-Based Induction Motor Drive Reliability under Different Control Schemes and Safe-Mode Operation

Ali M. Bazzi, Xiangyu Ding, Alejandro Dominguez-García, and Philip T. Krein
Grainger Center for Electric Machinery and Electromechanics
Department of Electrical and Computer Engineering
University of Illinois at Urbana-Champaign
Urbana, IL
{abazzi2, ding3, aledan, krein}@illinois.edu

***Abstract*—This paper proposes a reliability modeling method for induction motor drives based on an equivalent dq0 circuit model. The machine input voltages or currents are modeled as sources dependent on states and commands. This enables reliability analysis for different control strategies. The method utilizes failure modes and effects analysis, Monte Carlo simulations, and Markov models. Different controllers, in addition to faults in the machine, power electronics, and sensors, are addressed. The control methods considered in the analysis include constant volts per hertz (V/f), indirect field-oriented control (IFOC), direct torque control (DTC), and feedback linearization control (FLC). Direct line operation (DLO) is also considered. The proposed circuit-based reliability modeling method is versatile and easy to implement in commercial circuit simulators. The simulation model, which is experimentally verified, uses a reliability tool to evaluate the mean time to failure (MTTF) of the drive. Results show that, as expected, V/f control has the highest MTTF, due to its independence from sensor feedback, but poor dynamics. Among the closed-loop controllers, IFOC and DTC are better for fast dynamics, simplicity, and acceptable MTTF, but FLC is shown to have the longest MTTF. A safe-mode control scheme is proposed under which the drive is shown to have an even longer MTTF than V/f.**

***Keywords*—Motor drive reliability, safe mode controller , back-up controller induction motor drives, faults in motor drives, reliability enhancement.**

I. INTRODUCTION

Advanced induction machine applications, e.g., vehicles, aircraft oil pumps, and driving conveyors, require careful designs for safety and reliability. High reliability can be achieved through several approaches, e.g., multi-phase machines [1], sensorless control algorithms [2], fault tolerance [3], etc. While closed-loop motor control provides better dynamic performance than open-loop, sensor feedback poses a reliability concern if no fault tolerance or back-up controls are implemented. Thus, it is important to identify which closed-loop controller will provide the best performance and highest reliability under faults. Open-loop controllers, such as constant Volts-per-Hertz (V/f), require no sensors but have poor dynamic performance. Combining open- and closed-loop controls in a safe-mode arrangement is expected to produce high reliability and good dynamic performance. A versatile simulation tool is required to evaluate the reliability of different motor control schemes. This prevents damage to an experimental setup; allow easy controller replacement and automation of the fault impact assessment. To simultaneously study physical effects and fault transients in the machine, power electronics and sensing requires that the simulation tool runtime be reasonable. Some of the available literature addresses motor drives reliability models in non-circuit-based methods [4], but the model requires significant modifications to simulate new control laws. Other methods and reliability models have been elaborated upon in [4] and show a need for a versatile reliability evaluation tool, especially when motor drive controllers are compared.

This paper proposes a circuit-based reliability modeling and analysis approach of an induction motor drive under open- and closed-loop control. This approach shows that a safe-mode topology enhances overall drive reliability. It is promising because modeling electrical faults is straightforward in a circuit simulation environment, flexible in modeling different controllers, and easy to implement in circuit-based simulators. The reliability tool developed here performs fault simulations and evaluates the mean time to failure (MTTF) of the drive system. For every controller, the reliability modeling approach runs an automated fault modes and effects analysis (FMEA) that covers the effects of three consecutive faults on the drive. The machine model used is shown in Fig. 1 [5] where the dotted lines show the connection that can be modified to reflect current-fed or voltage-fed control strategies. Dependent current or voltage sources are used to mimic the controller operation. Motor drive controllers usually set a desired input current or voltage that depends on commands and maybe feedback. The

flexibility of this model lies in easy replacement of the equations controlling these dependent sources.

Section II describes the open- and closed-loop controllers in the stationary, synchronous, or rotor reference frames. Section III elaborates on the reliability tool in regard to the faults, failure rates, and the reliability evaluation procedure. Section IV shows the simulation model validation, and Section V presents the reliability evaluation of two open-loops and three closed-loop controllers. Section VI presents the proposed safe-mode control scheme, and Section VII concludes the paper.

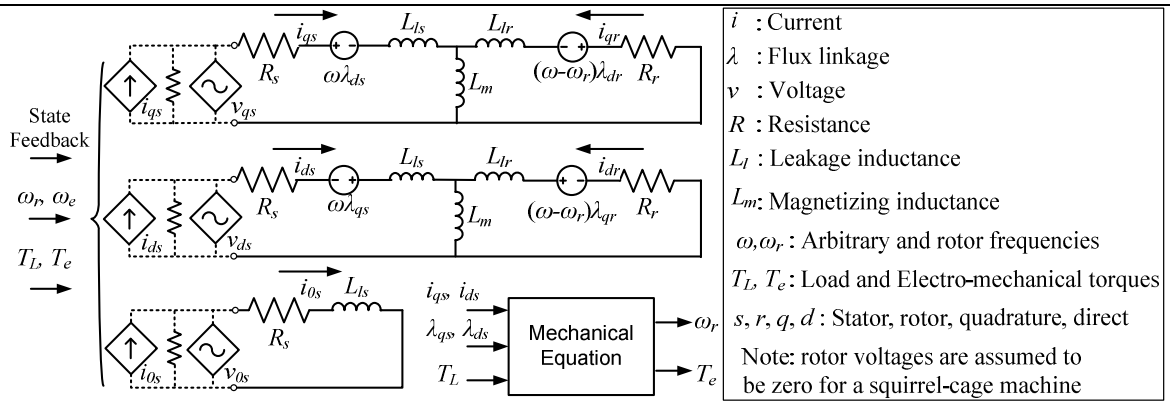

Fig. 1. Circuit-based induction motor model with control laws lumped into dependent sources

II. Motor Controllers

The *dq0* model shown in Fig. 1 is commonly used in induction motor control design. This model was used for two reasons: 1) most closed-loop controllers are designed in the dq0 frame, and 2) the model reference frame can be easily modified by changing ω. All required feedback signals are assumed to be available through sensors or estimators. Dependent sources were added to the model to mimic operation of different controllers. Open-loop direct-line operation (DLO) and constant volts per hertz control (V/f), in addition to three closed-loop controllers, are studied in the reliability analysis. The goals for analyzing both open- and closed-loop controllers are to find the best controllers and to study the safe-mode configuration where the open-loop runs as a backup for the closed-loop. The DLO is expected to have very low reliability as it runs at a single speed, but it has been widely used when electronic drives are not employed. The V/f is expected to have high reliability as it requires no sensor feedback. However, the dynamic response to load changes is generally worse than any closed-loop controller. The closed-loop controllers are indirect field-oriented control (IFOC), direct torque control (DTC), and feedback linearization control (FLC), and they are all expected to have acceptable reliability and good dynamic performance due to the corrective effects of feedback.

V/f [6] and DTC [7] are modeled in the stationary reference frame; IFOC [5] is modeled in the synchronous reference frame; and FLC [8] is modeled in the rotor reference frame. Block diagrams of all controllers, except DLO, are shown in Figures 2–5 where ω_e and ω_m are the electrical and mechanical frequencies, respectively; ψ_r is the rotor flux magnitude, * superscripts stand for commands, and *K*s are fractions of the inverter dc bus voltage.

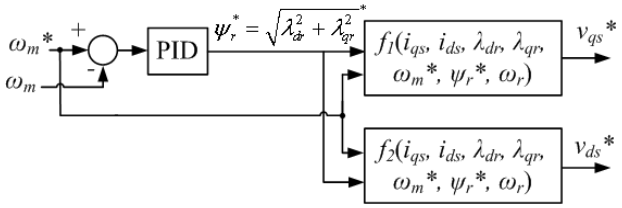

Fig. 2. IFOC in the synchronous reference frame

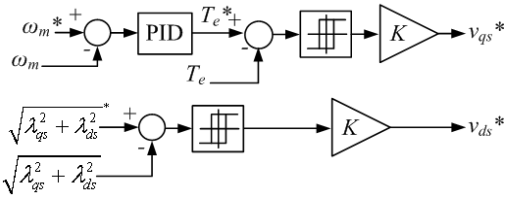

Fig. 3. DTC with torque and flux hysteresis

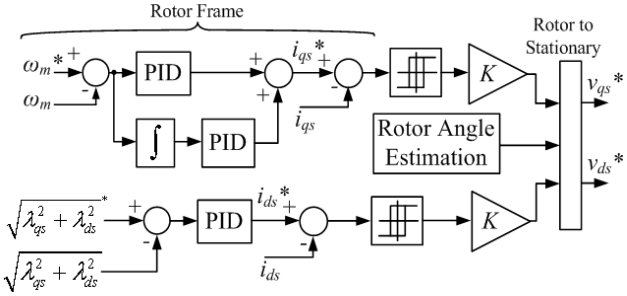

Fig. 4. FLC in the rotor reference frame

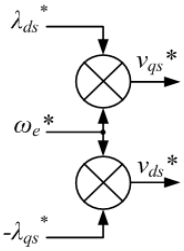

Fig. 5. Open-loop V/f control

The parameters λ_{dr} and λ_{qr} are rotor flux values; T_e is electrical torque and v_{ds}, v_{qs}, i_{ds}, i_{qs} are stator voltages and currents. Equations f_1 and f_2 in Fig. 2 are shown in (1) and (2) and were derived in [6]. Machine parameters are assumed to be well-known. Readers can refer to [9] for more details on parameter sensitivity of different drive controllers.

$$v_{qs} = \sigma_L \left(\begin{array}{l} n_p \omega_r i_{ds} + \frac{R_{lr}}{L_{lr}} L_m i_{ds} \frac{\left(i_{qs}\lambda_{dr} - i_{ds}\lambda_{qr}\right)}{\lambda_{qr}^2 + \lambda_{dr}^2} \\ + \frac{\lambda_{dr}}{\sqrt{\lambda_{qr}^2 + \lambda_{dr}^2}} u_{speed} + \frac{\lambda_{qr}}{\sqrt{\lambda_{qr}^2 + \lambda_{dr}^2}} u_{flux} \end{array} \right) + \frac{L_m}{L_{lr}} n_p \omega_r \lambda_{dr} \quad (1)$$

$$v_{ds} = \sigma_L \left(\begin{array}{l} -n_p \omega_r i_{qs} - \frac{R_{lr}}{L_{lr}} L_m i_{qs} \frac{\left(i_{qs}\lambda_{dr} - i_{ds}\lambda_{qr}\right)}{\lambda_{qr}^2 + \lambda_{dr}^2} \\ - \frac{\lambda_{qr}}{\sqrt{\lambda_{qr}^2 + \lambda_{dr}^2}} u_{speed} + \frac{\lambda_{dr}}{\sqrt{\lambda_{qr}^2 + \lambda_{dr}^2}} u_{flux} \end{array} \right) - \frac{L_m}{L_{lr}} n_p \omega_r \lambda_{qr} \quad (2)$$

In (1) and (2), n_p is the number of pole pairs; u_{flux} and u_{speed} are the flux and speed commands. The rest of the parameters are same as in Figures 2-5. Note that for all controllers shown in Figures 2–5, voltage control is utilized. Thus, dependent voltage sources controlled by equations that are modeled by the block diagrams are used in the simulations.

III. Reliability Modeling Procedure

A. Proposed Procedure

The reliability modeling procedure is used to study the fault impact on the drive performance and to calculate the reliability function $R(t)$ and its corresponding MTTF. The proposed procedure combines FMEA and Markov reliability modeling. It can be summarized as follows:

1. Identify, model, and assess the failure rates of possible faults.
2. Set desired system performance requirements.
3. Inject faults and assess system performance.
4. Identify system states after every fault and build Markov model or state diagram.
5. Assign failure and recovery rates to all branches in the diagram.
6. Build state-transition matrix $\mathbf{\Phi}$ and eliminate rows and columns of absorbing states.
7. Solve (3) to find the state transitioning probabilities.
8. Solve (4) to find $R(t)$.
9. Solve (5) to find the MTTF.

Equations (3)–(5) are fundamental in determining the transitioning probabilities and the drive reliability. In (3), the column vector $\mathbf{P}^T(t)$ includes the probability of occurrence of every fault sequence. $\mathbf{\Phi}$ is usually sparse as not all states are connected. Therefore, solving (3) is simple with computer tools. The initial probability vector, $\mathbf{P}^T(0)$, is a zero-vector except for the initial state before any fault occurs—this term is one.

$$\mathbf{P}^T(t) = e^{\mathbf{\Phi}^T t} \mathbf{P}^T(0) \quad (3)$$

With $\mathbf{\Phi}$ including transitions among K non-absorbing states only, i.e., states without permanent failure, these probabilities are summed to find the overall drive reliability. The MTTF is then found as the integral of $R(t)$. Note that the expected drive reliability at any time t can be found by simply evaluating $R(t)$.

$$R(t) = \sum_{i=0}^{K} P_i(t) \quad (4)$$

$$\text{MTTF} = \int_0^\infty R(\tau) d\tau \quad (5)$$

Reference [10] includes the detailed mathematical foundations of the reliability modeling and analysis procedure.

B. Reliability Analysis Tool

To implement the proposed procedure, a MATLAB/Simulink® tool was developed. This tool performs Monte Carlo experiments, where faults are randomly injected. The system dynamic response after the fault occurrence is recorded and evaluated according to predetermined criteria or performance requirements. Faults in sensors are considered as shown in [4], while electrical faults are modeled by modifying the circuit model shown in Fig. 1. For example, rotor over-temperature changes the rotor resistance, which changes the value of R_r. The reliability tool also computes fault coverage—the probability of the drive surviving a fault over a required speed range for a preset number of input steps. The input used here for the fault coverage study is the speed command. The truncation level—defined as the number of fault levels that can occur sequentially prior to total failure—is chosen to be three. In a fault sequence, only one fault per component occurs, and failure modes for each component are assumed to be independent. For example, a short circuit on the stator side will not cause a rotor bar to break, and vice versa. Different fault sequences are generated as permutations. For every sequence, the tool

checks whether the system meets the performance requirements. Performance requirements are preset to determine whether the system functions or fails. Finally, the state transition matrix is computed, the survivor function $R(t)$ is plotted, and the overall system mean time to failure (MTTF) is calculated. The pseudo-code of the tool is shown in Fig. 6.

```
Start Program
  Initialize model and input
  State = 1 C(1) = 1 (C(x) is the fault coverage for state x)
  State = 2
    for truncation level = 1 to 3
      for each state m in previous truncation level
        if C(x) > 0
          for each fault injection block without fault injected
            Generate fault sequence for current state
            for each surviving input combination
              Simulate system, inject fault sequence
                Check if system survives
            end for
            Compute fault coverage for present state
            State = State + 1
          end for
        end if
      end for
    end for
  Generate state transition matrix
  Find and plot R(t)
End Program
```

Fig. 6. Pseudo-code of the reliability analysis tool

C. Faults, Failure Rates, and Performance Requirements

Faults similar to those shown in [4] are utilized here and include most major faults that could occur in the machine, power electronics, and sensors (current sensors and speed encoder). In the simulation model, fault injection blocks have two variables: fault modes and failure rates. The fault mode is a Boolean parameter that is either 0 (No Fault) or 1 (Fault). Components with several fault modes, e.g., sensors, have multiple fault injection blocks. For this drive, 11 fault modes were implemented and are summarized in Table I.

TABLE I. FAULT MODES AND FAILURE RATES

Power electronics and machine faults (λ in Failures/hour)	
Rotor over-temperature	$\lambda_{ROT} = 5\times10^{-7}$
Broken rotor bar	$\lambda_{BRB} = 5\times10^{-7}$
b-c Phase-to-phase short circuit	$\lambda_{PP} = 3.2\times10^{-6}$
Phase *a* short circuit to ground	$\lambda_{SCG} = 5\times10^{-7}$
Phase *a* open circuit	$\lambda_{OC} = 5\times10^{-7}$
A-Phase current sensor faults	
Bias = + 1 A	$\lambda_{CSB} = 1\times10^{-7}$
Constant = 1 A	$\lambda_{CSC} = 1\times10^{-7}$
Gain = ×1.5	$\lambda_{CSG} = 1\times10^{-7}$
Omission	$\lambda_{CSO} = 1\times10^{-7}$
Speed encoder fault	
Constant = 1430 RPM	$\lambda_{SEC} = 1.9\times10^{-7}$
Gain = ×1.5	$\lambda_{SEG} = 1.9\times10^{-7}$
Omission	$\lambda_{SEO} = 7.4\times10^{-7}$

In Table I, power electronics and machine faults have been surveyed from common literature. Sensor faults shown are similar to those in [4, 11]—Gain: incorrect gain due to a sensor or interface circuit malfunction; Constant: Sensor or interface circuit saturation; Bias: incorrect shifting caused by the sensor interface circuit; Omission: zero output where sensor signal is shorted to ground or digital encoder malfunctions. Two types of fault injection blocks were implemented—circuit faults and signal faults. Both have a similar structure where the pre-fault dynamics and the post-fault dynamics are fed into two separate inputs of a multiplexer. The Boolean fault mode determines whether or not a fault is injected in each component. Fault injection blocks in the induction motor and power electronics are built using two ideal switches as shown in Fig. 7. The signal fault injection blocks are implemented using switch blocks as shown in Fig. 8.

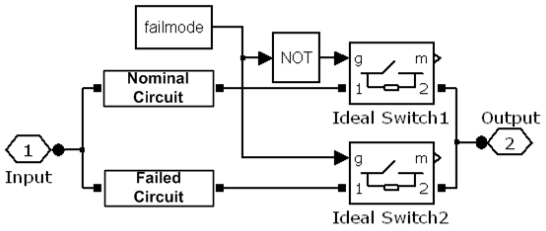

Fig. 7. Circuit fault injection block

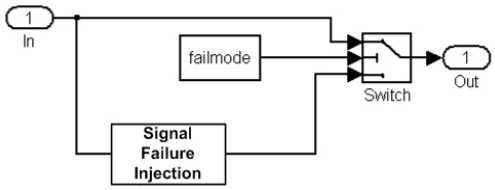

Fig. 8. Sensor fault injection

Faults that occur in the *abc* frame are transformed to the *dq0* frame to be consistent with the machine model. In general, the transformation between *abc* to *dq0* can be formulated for a variable *f* as shown in [5]

$$f_{qd0} = K_s f_{abc}, \tag{6}$$

where K_s matrix is given by

$$K_s = \frac{2}{3}\begin{bmatrix} \cos\theta & \cos(\theta-\frac{2\pi}{3}) & \cos(\theta+\frac{2\pi}{3}) \\ \sin\theta & \sin(\theta-\frac{2\pi}{3}) & \sin(\theta+\frac{2\pi}{3}) \\ \frac{1}{2} & \frac{1}{2} & \frac{1}{2} \end{bmatrix},$$

and the arbitrary reference speed is $\omega = d\theta/dt$. In the stationary reference frame, $\theta = 0$ and K_s can be simplified to

$$K_s = \frac{1}{3}\begin{bmatrix} 2 & -1 & -1 \\ 0 & -\sqrt{3} & \sqrt{3} \\ 1 & 1 & 1 \end{bmatrix}.$$

CSO in the stationary frame is derived here as an example. In the case of CSO, the currents are given by

$$\begin{bmatrix} I_a \\ I_b \\ I_c \end{bmatrix} = \begin{bmatrix} I_q \\ -\frac{1}{2}I_q - \frac{\sqrt{3}}{2}I_d \\ -\frac{1}{2}I_q + \frac{\sqrt{3}}{2}I_d \end{bmatrix}. \quad (7)$$

For omission in the *a*-phase current sensor, the current feedback for I_a is set zero. The faulted equation is transformed to the *dq0* frame using (7) and the fault in this frame can be modeled as

$$\begin{bmatrix} I_q^o \\ I_d^o \\ I_0^o \end{bmatrix} = \frac{1}{3}\begin{bmatrix} -2 \\ 0 \\ -1 \end{bmatrix} \times I_q + \begin{bmatrix} I_q \\ I_d \\ I_0 \end{bmatrix}, \quad (8)$$

where I_d^o, I_q^o, and I_0^o are the stator currents in the *dq0* stationary frame. Examples of fault transformations are shown in Table II. In Table II, I_q^x, I_d^x, I_0^x are post-fault current values and I_q, I_d, I_0 are the pre-fault values, where *x* is *g* for gain, *b* for bias, *o* for omission, *c* for constant and *O* for open circuit. Similar notation is used for the voltages.

TABLE II
dq0 FRAME FAULT MODELS

Phase *a* OC: V_a=0	Phase *a* CSG: I_a=*k* I_a
$\begin{bmatrix} V_q^O \\ V_d^O \\ V_0^O \end{bmatrix} = \frac{2}{3}\begin{bmatrix} -1 \\ 0 \\ -\frac{1}{2} \end{bmatrix} \times V_q + \begin{bmatrix} V_q \\ V_d \\ V_0 \end{bmatrix}$	$\begin{bmatrix} I_q^g \\ I_d^g \\ I_0^g \end{bmatrix} = \frac{2}{3}\begin{bmatrix} (k-1) \\ 0 \\ \frac{1}{2}(k-1) \end{bmatrix} \times I_q + \begin{bmatrix} I_q \\ I_d \\ I_0 \end{bmatrix}$
Phase *a* CSB: I_a= I_a+*B*	**Phase *a* CSC: I_a= *C***
$\begin{bmatrix} I_q^b \\ I_d^b \\ I_0^b \end{bmatrix} = \frac{2}{3}\begin{bmatrix} B \\ 0 \\ \frac{1}{2}B \end{bmatrix} + \begin{bmatrix} I_q \\ I_d \\ I_0 \end{bmatrix}$	$\begin{bmatrix} I_q^c \\ I_d^c \\ I_0^c \end{bmatrix} = \frac{2}{3}\begin{bmatrix} (C-I_q) \\ 0 \\ \frac{1}{2}(C-I_q) \end{bmatrix} + \begin{bmatrix} I_q \\ I_d \\ I_0 \end{bmatrix}$

Failure rates (failure/hour) shown in Table I are obtained from open-access literature such as [10, 12]. Note that the same fault modes and failure rates are used in all drives except for current sensor and speed encoder faults which are ignored in open-loop controllers. There is no claim of failure rate accuracy, but failure rates are common among all five controllers for comparison purposes. Knowing the orders of the failure rates, e.g., 10^{-7} failures/hour, is sufficient to find a reasonable reliability estimate.

Performance requirements are essential in determining whether the system survives or fails after a fault occurs. The requirements used in this study are shown in Table III. Note that the choice of these requirements definitely affects the reliability evaluation, e.g., setting the settling time to be very long gives the drive longer time to recover from a fault and thus some failures might not occur.

TABLE III
PERFORMANCE REQUIREMENTS

Performance requirement	Value
Torque & speed settling time	< 250 ms
steady-state speed error	< 72 RPM
steady-state torque error	< 1N·m
Current peak	< 50 A

IV. MODEL VALIDATION

Simulations provide a fast and safe environment to evaluate the drive reliability, but they need to be experimentally verified to validate their accuracy. The model in Fig. 1 was experimentally verified for both V/f and IFOC under several faults that do not cause catastrophic failures. Simulation and experiments utilize a prototype 1.5hp induction machine. Examples are shown in Figures 9–12.

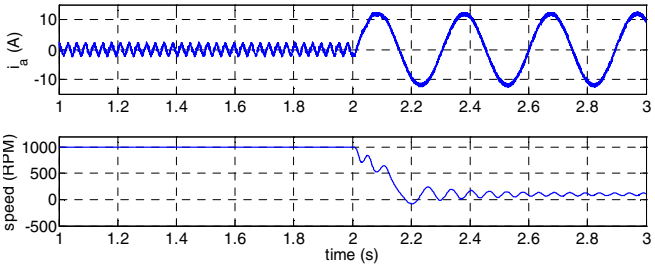

Fig. 9. Simulation results of IFOC under SEO

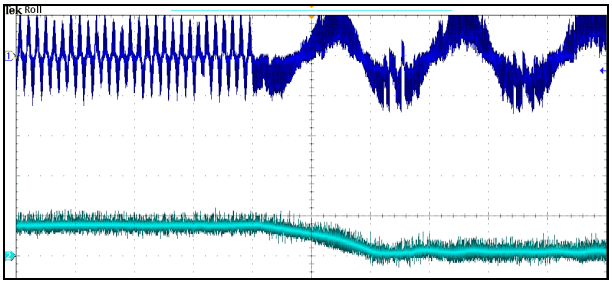

Fig. 10. Experimental result of IFOC under SEO: i_a (Top, 10 A/div), speed (bottom, 1000 rpm/div), time (200 ms/div)

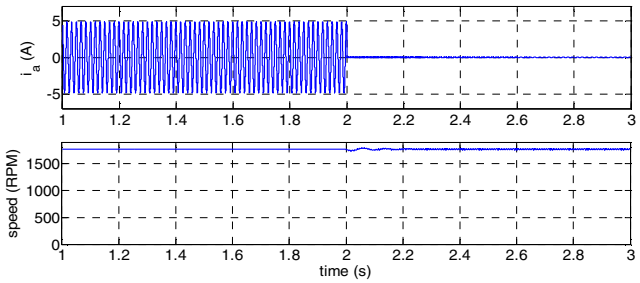

Fig. 11. Simulation result of V/f under OC in phase *a*

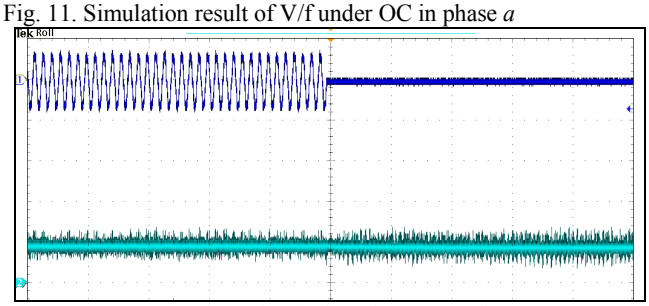
Fig. 12. Experimental result of V/f under OC in phase *a*: i_a (Top, 5 A/div), speed (bottom, 2000 rpm/div), time (200 ms/div)

Results show that the simulation response agrees with that of the experiments. In Figures 9 and 10, the drive fails under SEO as the speed drops below the desired command even though the current peaks remain within bounds. This is considered a failure because violating any of the performance requirements is considered as a system failure. Figures 11 and 12 show that once an OC occurs in phase *a*, the current drops to zero, but the speed is maintained as desired. Thus, the drive survived by operating only two phases, *b* and *c*, as none of the performance requirements are violated. Note that the general pre- and post-fault behaviors match well for these two examples. The simulation model behaves as expected from experiments. Thus, the simulation model is used hereafter to perform the reliability analysis. Note that in the simulation results shown, *dq0* currents from were transformed to the *abc* frame for comparison with measurements.

V. Reliability Results and Analysis

The reliability analysis procedure described in Section III-A was applied to the five controllers. Fault coverage over a wide speed range was studied. The reliability analysis tool along with the time-domain simulations of any drive evaluated the drive reliability in less than three hours. The runtime for V/f and DLO are especially fast since they do not consider sensor faults. This runtime is fast when considering three levels of faults and all possible fault permutations discussed in Section III-B. The overall runtime for all of the controllers did not exceed 12 hours. Thus, the proposed procedure and reliability tool are versatile for evaluating different controller and have a short runtime.

The two main outputs of the procedure described in Section III-A are $R(t)$ and the MTTF of the drive under a certain controller. The resulting $R(t)$s and MTTF's of the drive under the different controllers are shown in Fig. 13 where the top plot shows closed-loop drives, and the bottom plot shows the open-loop drive. As expected, V/f has the best reliability and highest MTTF as it is independent of sensors. While IFOC is slightly more reliable than DTC, FLC is the most reliable closed-loop controller, which can be attributed to its three PID loops that compensate for errors and maintain system operation. DLO is not reliable as it can only operate at the line frequency, so for a fault coverage study that considers 10 speed steps, the DLO automatically fails with a probability of 90%.

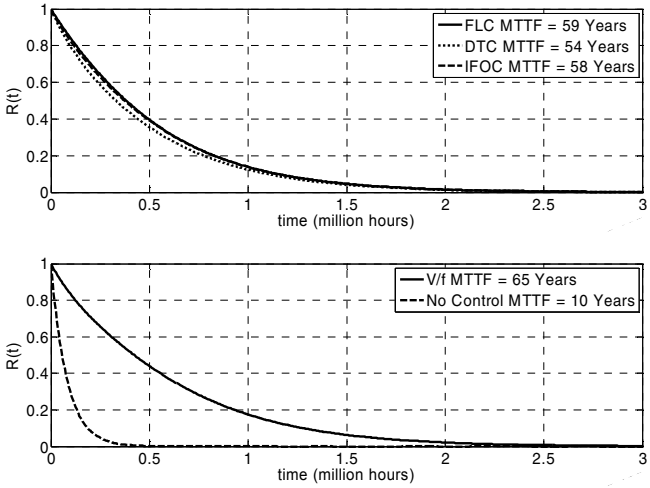

Fig. 13. R(t) and MTTF of the drive under different controllers

The MTTFs are also tabulated from highest to lowest in Table IV for convenience.

TABLE IV
Performance Requirements

Controller	Drive MTTF (years)
V/f	65
FLC	59
IFOC	58
DTC	54
DLO	10

The comparison of drive controllers would be incomplete if only the MTTF is used as the judging criterion. This is clear especially since the MTTFs of V/f, FLC, IFOC, and DTC are very close. Two other comparison criteria are addressed: the control complexity, and the dynamic response. From Figures 2–5, one can infer that V/f is the simplest, and DTC is the simplest among closed-loop controllers. The dynamic response of the drives under a speed step was compared for these four controllers, i.e., excluding DLO, and the results are shown in Fig. 14. It is evident in Fig. 14 that V/f has the worst dynamic response, while IFOC and DTC both have excellent performance.

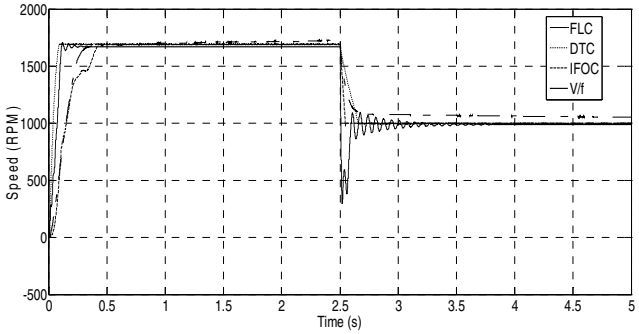

Fig. 14. Dynamic drive response for a load step

VI. Safe-Mode Operation

Closed-loop controllers have better dynamic performance when compared to open-loop controllers, and open-loop V/f has high reliability compare to its closed-loop counterparts. Thus, Combining both closed-loop and open-loop controls in a switched control system is expected to produce even higher reliability with excellent dynamic performance. The proposed configuration is to have the sensor-independent V/f run as a safe mode in parallel with the closed-loop controller. The safe mode is utilized once a sensor fault is detected. This system is shown in Fig. 15 where the closed-loop or "regular" controller is IFOC and the open-loop safe-mode is V/f. The choice of IFOC comes from the results in Section V where it was shown to be more reliable than DTC, less complex than FLC, and good dynamic performance.

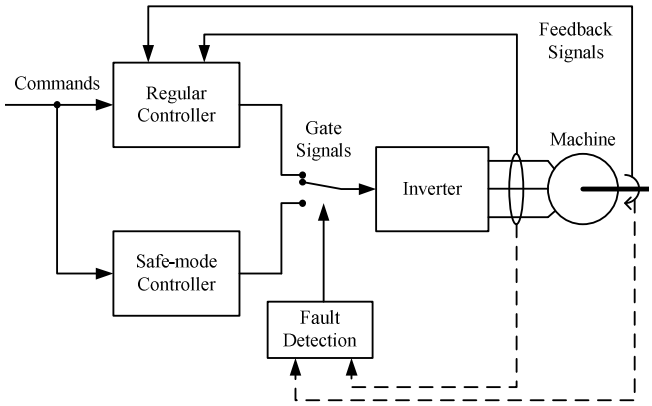

Fig. 15. Proposed safe-mode operation

The system shown in Fig. 15 is expected to have higher MTTF than both IFOC and V/f—V/f will mitigate sensor faults while the feedback control of IFOC will offer better reliability during other faults. In Fig. 15, the sensor fault detection circuitry is the decision maker in the switched control system. In this study, the fault detection circuitry is assumed to be ideal, i.e., it can detect a sensor fault instantaneously upon occurrence. One limit of a real fault detection circuit is the processing time or response delay time. This time, t_f, is expected to be within a few line-frequency periods. It is only during t_f that the system is affected by the sensor fault—there is no problem before the sensor fault occurs, and once V/f is engaged after t_f, the sensor fault no longer affects the system.

The drive reliability was evaluated for different values of t_f and the reliability functions are plotted in Fig. 16. It is clear that as t_f increases, the MTTF decreases because the drive will be operating for a longer time under the sensor fault. As expected, the MTTF of the proposed system is higher than that of V/f or IFOC, and the drive reliability increases to over 71 years compared to 58 and 65 years of IFOC and V/f, respectively.

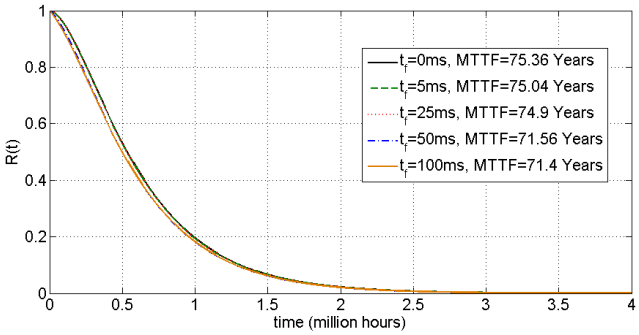

Fig. 16. Effect of delay switching time on the proposed safe-mode scheme

It is important to mention that adding the safe-mode controller does not significantly increase the system cost, especially when digital control is utilized. This is true as the two controllers can be programmed into the same drive controller chip. The only incurred cost is that of the fault detection circuitry which is expected to be insignificant whether being analog or digital. Thus, this safe-mode configuration offers significant increase in the drive reliability while maintaining IFOC dynamic performance except under sensor faults.

VII. Conclusion

This paper presented a versatile circuit-based reliability modeling procedure and reliability evaluation tool. The proposed procedure is straightforward and can be extended or reduced to study more or less faults in the system. The circuit-based modeling provides the flexibility of changing the drive controller and re-evaluating the drive reliability without significant changes to the simulation model. The simulation model utilized was verified experimentally, and results show that open-loop V/f has the highest reliability at the cost of poor dynamic performance. Closed-loop controllers were shown to have acceptable reliabilities which can be improved by reducing the sensor fault impact. Thus, a safe-mode scheme was proposed and results show that it is significantly more reliable. The effect of the sensor fault detection delay was also studied where as the the delay increases, the drive MTTF decreases. Further research on the sensor fault detection circuit or subsystem is part of the intended future work.

REFERENCES

[1] E. Levi, R. Bojoi, F. Profumo, H. A. Toliyat, and S. Williamson, "Multiphase induction motor drives - a technology status review," *IET Elect. Power Appl.,* vol. 1, pp. 489 - 516 2007.

[2] B. W. Williams, J. K. Goodfellow, and T. C. Green, "'Sensorless' speed measurement of inverter driven squirrel cage induction motors," in *Proc. Int. Conf. on Power Electron. and Variable-Speed Drives*, 1990, pp. 297 - 300

[3] A. M. S. Mendes and A. J. M. Cardoso, "Fault-tolerant operating strategies applied to three-phase induction-motor drives," *IEEE Trans. Ind. Electron.,* vol. 53, pp. 1807 - 1817 2006.

[4] A. M. Bazzi, A. Dominguez-Garcia, and P. T. Krein, "A method for impact assessment of faults on the performance of field-oriented control drives: A first step to reliability modeling," in *Proc. IEEE Appl. Power Electron. Conf. and Expo.*, 2010, pp. 256 - 263

[5] P. C. Krause, O. Wasynczuk, and S. D. Sudhoff, *Analysis of Electric Machinery and Drive Systems*, 2nd ed. New York: Wiley - IEEE Press, 2002.

[6] P. T. Krein, F. Disilvestro, I. Kanellakopoulos, and J. Locker, "Comparative analysis of scalar and vector control methods for induction motors," in *Proc. IEEE Power Electron. Specialists Conf.*, 1993, pp. 1139 - 1145.

[7] Z. Sorchini and P. T. Krein, "Formal derivation of direct torque control for induction machines," *IEEE Trans. Power Electron.,* vol. 21, pp. 1428 - 1436 2006.

[8] R. Marino, I. Kanellakopoulos, and P. Kokotovic, "Adaptive tracking for feedback linearizable SISO systems," in *Proc. IEEE Conf. on Decision and Control*, 1989, pp. 1002-1007.

[9] A. M. Bazzi, A. P. Friedl, S. Choi, and P. T. Krein, "Comparison of induction motor drives for electric vehicle applications: Dynamic performance and parameter sensitivity analyses," in *IEEE Int. Electric Machines and Drives Conf.*, 2009, pp. 639-646.

[10] "Military Handbook Reliability Prediction of Electronics Equipment," MIL-HDBK-217F, Department of Defense 1995.

[11] A. D. Dominguez-Garcia, "An integrated methodology for the performance and reliability evaluation of fault-tolerant systems," Cambridge, MA: Ph.D. Thesis, Massachusetts Institute of Technology, June 2007.

[12] "IEEE standard reliability data for pumps and drivers, valve actuators, and valves " ANSI/IEEE Std 500 1984.